Chapter 2
Force Spectroscopy of DNA and RNA: Structure and Kinetics from Single-Molecule Experiments

Rebecca Bolt Ettlinger, Michael Askvad Sørensen, and Lene Broeng Oddershede

Abstract Force spectroscopy of individual DNA and RNA molecules provides unique insights into the structure and mechanics of these for life so essential molecules. Observations of DNA and RNA molecules one at a time provide spatial, structural, and temporal information that is complementary to the information obtained by classical ensemble methods. Single-molecule force spectroscopy has been realized only within the last decades, and its success is crucially connected to the technological development that has allowed single-molecule resolution. This chapter provides an introduction to in vitro force spectroscopy of individual DNA and RNA molecules including the most commonly used techniques, the theory and methodology necessary for understanding the data, and the exciting results achieved. Three commonly used single-molecule methods are emphasized: optical tweezers, magnetic tweezers, and nanopore force spectroscopy. The theory of DNA stretch and twist under tension is described along with related experimental examples. New principles for extracting kinetic and thermodynamic information from nonequilibrium data are outlined, and further examples are given including the opening of DNA and RNA structures to reveal their energy landscape. Finally, future perspectives for force spectroscopy of DNA and RNA are offered.

Contents

R.B. Ettlinger • L.B. Oddershede (✉)
The Niels Bohr Institute, University of Copenhagen, Copenhagen, Denmark
e-mail: rebecca@nbi.dk; oddershede@nbi.dk

M.A. Sørensen
The Department of Biology, University of Copenhagen, Copenhagen, Denmark
e-mail: mas@bio.ku.dk

Nomenclature

ΔG	Gibbs free energy change
$\Delta G^{\ddagger}$	Activation energy
CFT	Crooks fluctuation theorem
dsDNA	Double-stranded DNA
EWLC	Extensible worm-like chain model
FJC	Freely jointed chain model
JE	Jarzynski equality
$k(F)$	Rate of transition at force F
k_0	Rate of transition at zero force
K_0	Elasticity
L_c	Contour length
L_p	Persistence length
MT	Magnetic tweezers
NFS	Nanopore force spectroscopy
OT	Optical tweezers
ssDNA	Single-stranded DNA
TWLC	Twistable worm-like chain model
WLC	Worm-like chain model
$x^{\ddagger}$	Distance to the transition state

2.1 Introduction

The response of single DNA and RNA molecules to force helps reveal their structure and the transitions they undergo when experiencing mechanical stress. In essence, molecular force spectroscopy probes how molecules comply with tension. Experimenters uncover molecular response over a range of pulling forces or a range of degrees of twist. They may also study the molecular response at a constant force for an extended period of time. The results provide information about the mechanical deformation that DNA and RNA may experience in other contexts, e.g., due to enzyme binding, artificial manipulation, or strand separation during cell division. This makes molecular force spectroscopy a crucial tool in nucleic acids nanotechnology.

The present chapter focuses on in vitro single-molecule force spectroscopy investigations of DNA and RNA. Examples include stretch-induced melting of double-stranded DNA (Sect. 2.3.1), mapping the energy landscape of DNA hairpins (Sect. 2.5.2), and exploring how mRNA pseudoknots unfold (Sect. 2.5.3). One major field not covered here is the use of force spectroscopy to examine the action of enzymatic complexes such as RNA polymerase and ribosomes on polynucleic acids. Recent reviews of this area have been made by, e.g., Bryant et al. (2012) and Lavelle et al. (2011). Another field omitted here is in vivo single-molecule force spectroscopy, which has recently been reviewed by Oddershede (2012).

Early pulling experiments on individual molecules of DNA and RNA have shown that the intrinsic nature of these polymers is more like that of a "worm-like chain," i.e., a continually flexible elastic cord, than a "freely jointed chain" with stiff linkers oriented at random (Bustamante et al. 1994). The flexibility and elasticity of single-stranded RNA and single- and double-stranded DNA (ssDNA and dsDNA) have been evaluated (Mangeol et al. 2011; Chen et al. 2012; Wang et al. 1997), and DNA response to twist and the coupling between stretching and twisting have been quantified (Gore et al. 2006; Gross et al. 2011). Further experiments have extensively probed the overstretching transition of double-stranded DNA where a 70 % increase in length is suddenly observed at high force; the exact force at which the transition takes place varies, e.g., with pH (Cluzel et al. 1996; Williams et al. 2001).

Force spectroscopy has further been used to illuminate patterns of bond breakage and formation, as pulling can alter the chemical structure of the molecule being examined. Classical studies include the unzipping of the strands of dsDNA and the unfolding of RNA hairpins, both of which are accompanied by identifiable changes in molecular extension directly related to the number of base pairs opening (Essevaz-Roulet et al. 1997; Liphardt et al. 2001). Data on transition forces and molecular extension at a given force have allowed evaluation of the brittleness and strength of the structure being pulled. These data also provide access to the rate of formation and dissociation at zero force (Liphardt et al. 2001) and the Gibbs free energy change of the transition (Liphardt et al. 2002; Collin et al. 2005).

The following section introduces the three most commonly used methods for force spectroscopy of DNA and RNA: optical tweezers, magnetic tweezers, and nanopore force spectroscopy. Section 2.3 of this chapter describes the characterization of DNA response to stretch and twist, while Sects. 2.4 and 2.5 lay out the principles developed within the last 15 years to extract kinetic and thermodynamic parameters from transition data. Several notable experimental results are shown. Finally, Sect. 2.6 provides a summary and perspectives on what to expect from force spectroscopy of DNA and RNA in the coming years.

2.2 Commonly Used Methods

Three main methods of molecular force spectroscopy are described in this section: optical tweezers, magnetic tweezers, and nanopore force spectroscopy (OT, MT, and NFS). When using optical and magnetic tweezers, the experimenter applies force to the molecule under investigation by tethering it between extremities such as artificial beads that can be manipulated with the instrument. Calibration allows conversion of the measurement output to force. In nanopore force spectroscopy, a difference in electrical potential pulls single molecules across a membrane, requiring no external attachment of the molecule under investigation, but also providing no direct measurement of the magnitude of the force. The three approaches are illustrated in Fig. 2.1 and compared in Table 2.1.

Other force spectroscopy techniques that have been applied to DNA and RNA include atomic force microscopy (AFM) (Strunz et al. 1999), microneedle manipulation (Essevaz-Roulet et al. 1997), and application of flow to tethered molecules (Perkins et al. 1997). AFM most efficiently probes at higher forces than the structural transitions of polynucleic acids and is more commonly used to investigate protein filaments. Microneedle manipulation gives access to lower forces than AFM, but accurate measurements are difficult to obtain. Application of flow allows measurement of both molecular extension and molecular flexibility in a buffer that is easily exchanged, but force is not easily measured, and manipulative control is limited (Bustamante et al. 2000).

2.2.1 Optical Tweezers

An optical trap captures nanometer to micrometer-sized objects such as cells or highly refractive beads through the induction of an electrical dipole by a tightly focused laser beam. The interaction can be viewed as a balance between the scattering and gradient forces exerted by the laser. The scattering force pushes the object in the direction of the light's propagation, while the gradient force pulls it towards the point of greatest light intensity. A full analysis of these forces requires calculations which take into account the exact shape and size of the object
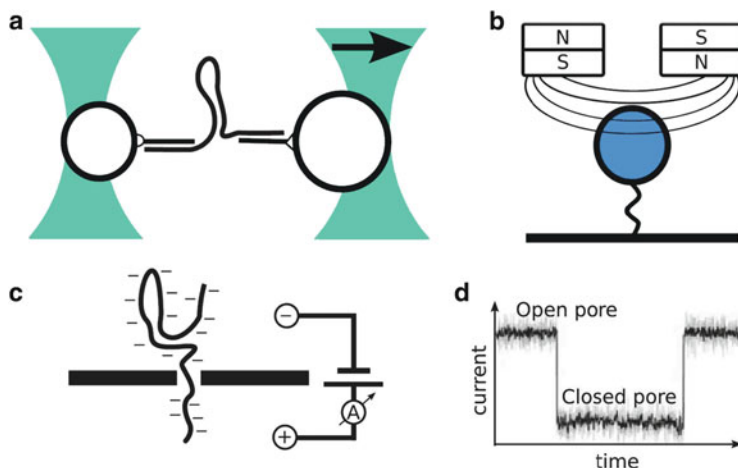
Fig. 2.1 Force spectroscopy methods. (**a**) Dual beam optical tweezers for pulling a single-stranded polynucleic acid hairpin. The single-stranded DNA or RNA molecule is attached to two single-stranded DNA handles via base pairing. The DNA handles are attached through linker molecules to the beads. (**b**) Simple magnetic tweezers for pulling and twisting a polynucleic acid attached through linkers to the sample chamber surface and to a magnetic bead. Figure inspired by de Vlaminck and Dekker (2012). (**c**) Nanopore force spectroscopy for investigating the structure of a single-stranded polynucleic acid. The electrical field across the membrane exerts a force on the negatively charged DNA or RNA molecule. The current through the membrane is monitored (**d**) as DNA passes and the amount of time that the pore is closed (the passage time) is used to characterize the unfolding of the single-stranded structure. Figure inspired by Dudko et al. (2010)

Table 2.1 Characteristics of the most common molecular force spectroscopy methods

	Typical force	Stiffness	Spatial resolution	Twist	Usage
OT	0.1–200 pN	0.005–1 pN/nm	0.1 nm	With permanent dipole in handles	Lateral and axial pull. Handles needed
MT	0.001–20 pN	$\approx 10^{-6}$ pN/nm	1 nm	Yes	Axial pull, torque measurement
					Magnetic handles needed
NFS	1–30 pN (solid-state nanopore)	≈ 0.2 pN/mV (solid-state nanopore) (Keyser et al. 2006)	NA	No	Axial pull across a membrane. No handles. No direct force/distance measurement

OT optical tweezers, *MT* magnetic tweezers, *NFS* nanopore force spectroscopy

(Rohrbach 2005). Here we will simply note that the force created by a focused laser with a Gaussian intensity profile can stably hold an object with an index of refraction larger than that of the surrounding medium. The trapping potential is

approximately harmonic with $F = -\kappa x$, where F is the force of the trap on the object, κ the trap stiffness, and x the displacement of the object from the trap center. The potential is strongest for objects about the size of the wavelength of the laser, often about 1 μm, and can extend several hundred nanometers, exerting forces of more than 100 pN.

A typical optical tweezers setup consists of a laser implemented in an inverted microscope which focuses the trapping laser on the sample using the microscope objective. The position of the object in the trap can be monitored either by video microscopy or by collecting the laser light by a condenser and focusing it onto a photodiode. The trap may be moved with optical devices such as galvanic mirrors or acousto-optical deflectors. In some cases, the trapping beam is split into several independently controlled traps. Calibration is based on measurement of the constrained Brownian motion of the bead in the trap, sometimes combined with drag measurements. This allows conversion of the voltage output from the photodiodes to precise measurements of position and force (Gittes and Schmidt 1998).

In force spectroscopy experiments, the DNA or RNA molecule under investigation is attached by linkers such as biotin–streptavidin or digoxigenin–antidigoxigenin bindings to two optically trapped beads, to a trapped bead and a surface, or to a trapped bead and a bead held by a micropipette. During experiments, the surface, the micropipette, or one of the optical traps may be moved in a controlled fashion in order to extend the molecule and apply force. Most often the force is either changed at an approximately constant rate (force ramp) or held constant by a feedback system.

The precise nature of the attachment between the molecule and the bead must be taken into account in interpretation of the results. For instance, rotational constraint can be crucial for the molecule's response to stretch. This may be determined by whether dsDNA is attached to the beads or to the surface by both strands or only by one strand (see Sect. 2.3.1). Single-stranded DNA or RNA under investigation is commonly attached by base pairing to single-stranded handles, which again are attached to linkers and beads (Fig. 2.1a). Any significant stretching of these handles must be included in the data analysis. This is especially relevant when evaluating, for instance, changes in molecular extension.

Long handles can make experimentation easier because the two points of attachment are better separated spatially, thus reducing surface interactions. Larger separation also reduces dual trap interference. Short handles on the other hand reduce noise and the contribution of handle stretching.

Optical tweezers are usually used for pulling experiments in which force is applied parallel to the axis between the two molecular points of attachment. In the last 10 years, however, optical torque wrenches have been introduced. These use polarized light to turn birefringent particles and thus twist molecules in the plane perpendicular to the direction of propagation of the laser (La Porta and Wang 2004). In combination with other techniques, optical tweezers thus enable a wide range of investigations into polynucleic acids and their interactions with other components of the cell. A review of the diverse capabilities and applications of optical tweezers in biomedicine is provided by Stevenson et al. (2010).

2.2.2 Magnetic Tweezers

The simplest magnetic tweezers consist of two movable magnets mounted above a sample chamber. The magnetic field creates a force on a magnetic bead, which can be moved relative to the sample chamber surface by moving either the chamber or the magnets. Torque can be applied by using paramagnetic beads, since the magnetic field induced in a paramagnet is stronger along one axis, which will align to the magnetic field. This ability to apply torque is a key advantage of magnetic tweezers. Another important property is that in contrast to optical tweezers, the force of magnetic tweezers does not change appreciably with bead movement in the trap. Thus, the force on the bead is more or less constant despite changes in, e.g., molecular extension. The near-constant magnetic field also means that magnetic tweezers exert force on all magnetic particles in the sample at the same time.

For force spectroscopy experiments, the molecule is frequently tethered between a magnetic bead and the sample chamber surface (Fig. 2.1b). The magnetic tweezers are usually built into a microscope, and detection of changes in extension of the molecule is done using CCD cameras. These cameras track the interference pattern created by the bead's motion with respect to the microscope focus. The CCD output is calibrated with a series of images of the bead at known z-heights above the sample chamber surface.

Force calibration is done by monitoring the Brownian motion of the tethered bead and invoking the equipartition theorem while applying knowledge of the extension of the molecule from the CCD images. To do this, the tether is treated as a pendulum with a lateral stiffness constant α_x, so that $\alpha_x = F_z/L$, where F_z is the upward force on the bead and L is the length of the tether (Neuman and Nagy 2008). The energy of the particle is related to the average bead displacement from the center of its movement by $k_BT = \alpha_x <x^2>$, where k_B is the Boltzmann constant and T the temperature, so that $F_z = Lk_BT/<x^2>$.

The magnitude of the torque applied to twist the molecule a given number of turns cannot be directly measured in most magnetic tweezers setups. However, using new techniques that allow almost unconstrained turning of the molecule, experimenters have been able to measure torque by measuring the average motion of fluorescent beads attached to the molecule or of marker beads attached to the magnetic bead. These and other recent technical advances in magnetic tweezers are reviewed by de Vlaminck and Dekker (2012).

2.2.3 Nanopore Force Spectroscopy

Nanopore force spectroscopy (NFS) is intrinsically different from OT and MT force spectroscopy because force is applied electrically rather than mechanically. Therefore, force is applied diffusely to the entire molecule rather than at a single point.

In a typical DNA or RNA NFS experiment, a nanopore just large enough for the passage of single-stranded DNA or RNA is located in a membrane that separates two buffer reservoirs (Fig. 2.1c). The pore may be either biological, e.g., an α-hemolysin pore in a lipid membrane, or solid state, e.g., etched in a silicon-based membrane. A voltage is applied across the membrane, and the current due to ion flow through the pore is measured. If a DNA or RNA molecule enters the pore, the current changes due to the change in ion flow (Fig. 2.1d). After a characteristic time, the molecule is pulled across the membrane by the voltage drop because both DNA and RNA have a net negative charge under physiological buffer conditions. The time that the DNA or RNA molecule takes to pass the membrane is monitored. The passage time data are used to extract kinetic parameters of the structural change, such as hairpin unfolding, that occurs while the molecule passes through the pore.

Unlike OT and MT force spectroscopy, NFS does not allow for direct measurement of force. However, the technique can be combined with optical trapping for accurate force measurements. Alternatively, one may approximate the force by calculating the estimated charge on the molecule, since $F = q_{eff}E$, where F is the force on the molecule, q_{eff} is the effective charge of the molecule inside the pore, and E is the electric field across the pore. Keyser et al. (2006) combined optical trapping and nanopore force spectroscopy and found $q_{eff} \approx 0.25Q$ for a variety of buffer strengths, where Q is the bare DNA charge.

NFS may allow easier access to large amounts of single-molecule force spectroscopy data than OT or MT, since it may be more efficient to coerce molecules through a membrane ion channel than to capture them one at a time with optical or magnetic traps. The high throughput of the technique has already proven useful in validating new theory for extracting kinetic rates of DNA hairpin unfolding (Sect. 2.4.3; Dudko et al. 2010).

2.3   Stretching DNA and RNA

How does DNA conform to force along its length and how elastic is it? Does the double-stranded helix unwind as it is pulled? And how do single-stranded DNA and RNA differ from double-stranded molecules in their response to tension?

The answers have important implications both for direct manipulation of DNA in nanotechnological applications and for understanding the action of DNA-modifying molecular motors that locally bend or stretch the molecule as they progress along their template. DNA stretching and twisting have therefore been investigated experimentally in vitro since the mid-1990s. Curves of applied force versus molecular end-to-end distance (Fig. 2.2a) show that dsDNA may be extended almost without resistance from an initially randomly coiled position until it approaches its contour length, L_c. The contour length is the molecule's extension when completely straightened but not stretched. Near the contour length, more and more force must be applied to further extend the molecule. Surprisingly, however,
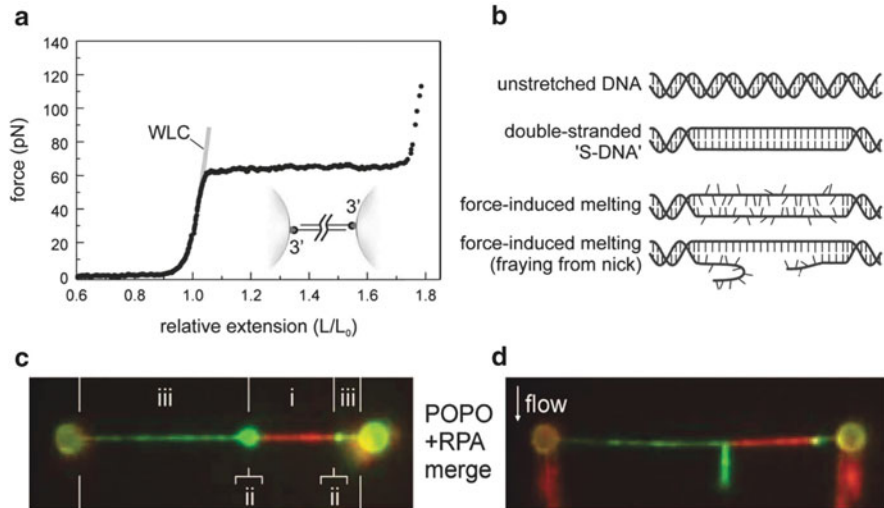
Fig. 2.2 dsDNA force–extension behavior: (**a**) Force–extension curve showing the overstretching transition at 65 pN for rotationally unconstrained dsDNA. The DNA is attached at the 3′ end of each strand as indicated in the *inset*. L_0 is the contour length, called L_c in the remainder of this chapter. (**b**) Hypothesized DNA conformations during the overstretching transition. (**c**) Overstretched λ-DNA held between two optically trapped beads. Attachment to beads as shown in *inset* in (**a**); note that the DNA is free to rotate. The same DNA is shown in (**c**) and (**d**). *Red*: dsDNA labeled with the fluorescent dsDNA-intercalator POPO-3. *Green*: ssDNA labeled by enhanced green fluorescent protein-tagged replication protein A (eGFP-RPA). (**d**) Flow is applied perpendicular to the extended molecule so that ssDNA is clearly seen flowing away from the remaining dsDNA. Reproduced with permission from van Mameren et al. (2009)

at high force, the force–extension curve of dsDNA displays an overstretching plateau at which the molecule can be lengthened by about 70 % beyond its contour length with very little resistance.

If the molecule is free to rotate, e.g., if the beads are attached only to one strand at each end of the double-stranded DNA, the overstretching plateau occurs at about 65 pN. In contrast, if the molecule is rotationally constrained because both strands are attached at both ends, the overstretching plateau occurs at around 110 pN (Leger et al. 1999).

2.3.1 The Nature of Overstretched DNA

The nature of the DNA structure at the overstretching plateau in the dsDNA force–extension curve has been the subject of controversy for over a decade. Two possibilities were put forward (Fig. 2.2b): (1) that the overstretching results from unwinding of the original double helix structure of dsDNA (B-DNA), creating a

ladder-like double-stranded structure ("S-DNA") (Cluzel et al. 1996), and (2) that the base pairs connecting the double strands of the B-DNA melt, creating two single strands (Williams et al. 2001).

These discussions were significantly advanced in 2009 by van Mameren et al. The group performed a series of pulling experiments combining optical tweezers and fluorescence imaging. Using a range of fluorescent markers that bind only to either double- or single-stranded DNA, and using two different methods of DNA attachment, they were able to show that the overstretching transition for rotationally unconstrained DNA at 65 pN occurs due to melting of the dsDNA strand into ssDNA (Fig. 2.2c, d). The melting was shown to initiate at a free end of the dsDNA or at a nicked site. Additionally, the group showed that if the dsDNA was rotationally constrained, then the overstretching plateau occurred at 110 pN.

The investigation and discussion of the structure of overstretched dsDNA is ongoing, and Zhang et al. (2012) recently showed that the nature of the DNA formed during the transition is dependent on temperature, buffer strength, and DNA base composition. The group observed two different types of overstretching transitions near 65 pN in rotationally unconstrained DNA. One corresponds to the melting into single strands observed by van Mameren et al. (2009) and occurs at relatively high temperatures (generally room temperature or above), low GC content, and/or low salt concentrations. The other transition, which occurs at lower temperatures, higher salt concentrations, and/or higher GC content, appears to correspond to a transition from B-DNA to a structure which is yet not structurally characterized but where the two strands of the original B-DNA do stay closely associated.

The experiments by van Mameren et al. (2009) were carried out at salt concentrations up to 150 mM NaCl, which corresponds to the observation of Zhang et al. (2012) that a melting transition occurs for dsDNA with up to 50 % GC content when pulled at room temperature in a buffer with less than 150 mM NaCl.

2.3.2   Models of DNA Stretch

To describe the force–extension properties of dsDNA at low forces, the worm-like chain (WLC) model is often used (Bustamante et al. 1994; Collin et al. 2005). This model treats the DNA as a rope or an electrical cord which at forces below about 10 pN can be stretched entropically (i.e., by changing its state of disorder without changing the internal energy or other enthalpy components). An interpolation formula for the WLC model uses the contour length, L_c, along with the characteristic persistence length, L_p, to predict the end-to-end distance, x, at a particular pulling force, F (Marko and Siggia 1995):

$$F = \frac{k_B T}{L_p}\left[\frac{1}{4(1 - x/L_c)^2} - \frac{1}{4} + \frac{x}{L_c}\right] \qquad (2.1)$$

The persistence length, L_p, indicates how easily the polymer is bent at a given temperature. It is directly proportional to the polymer's flexural rigidity, κ_f, and inversely proportional to temperature: $L_p = \kappa_f/k_B T$. The flexural rigidity, κ_f, is the product of Young's modulus, Y, a property that describes the inherent material stiffness, and the inertial cross section, J, which relates purely to the polymer's geometry (Boal 2002).

To better describe the behavior of dsDNA at pulling forces above 10 pN, the WLC model has been modified by the addition of a parameter characterizing the enthalpic elasticity, K_0, in the extensible worm-like chain (EWLC) model (Wang et al. 1997). This incorporates the stretching ability of the polymer's intrinsic structure. Both the WLC and the EWLC models have been used to characterize the stretching of ssDNA and RNA as well as dsDNA, though ssDNA is sometimes described by the freely jointed chain model and its true behavior may be a hybrid of EWLC and FJC behavior (Rouzina and Bloomfield 2001). Single-stranded molecules are more flexible than dsDNA with correspondingly lower L_p, but they are approximately as elastic, showing about the same K_0. For dsDNA, $L_p \approx 47$ nm, while for single-stranded RNA, $L_p \approx 1.5$ nm (Mangeol et al. 2011). The values vary with buffer strength, and while, for instance, $L_p \approx 0.75$ nm has been found for ssDNA in 150 mM NaCl by Smith et al. (1996), a range between 1 and 6 nm have been found for ssDNA using different measurement techniques in other buffers, mainly weaker ones. To complicate the picture, addition of divalent cations, e.g., magnesium, appears to increase the persistence length much more dramatically than increasing monovalent salt concentration (Chen et al. 2012; Bizarro et al. 2012).

Recently, the EWLC model for dsDNA has been improved for forces above 35 pN by taking into account the coupling between twist and stretch that occurs for rotationally unconstrained DNA as further discussed in Sect. 2.3.4. The twistable worm-like chain (tWLC) model fits the force–extension data accurately up to the overstretching plateau at about 65 pN, as seen in Fig. 2.3a. In addition to L_c, L_p, and K_0, the model incorporates the DNA's twist rigidity, C, and an empirically derived function, $g(F)$, describing the coupling of twist and stretch to predict the force–extension curve. The tWLC model is formulated as (Gross et al. 2011)

$$x = L_c \left(1 - \frac{1}{2}\sqrt{\frac{k_B T}{F L_p}} + \frac{FC}{-g(F)^2 + K_0 C} \right) \tag{2.2}$$

Importantly, the family of WLC models can only be applied when the contour length is much longer than the persistence length ($L_c \gg L_p$). The contour length of a dsDNA base pair at zero force is about 0.28 nm while that of a single-strand nucleotide is about 0.59 nm (Hansen et al. 2007). Thus, for the WLC models to apply, the dsDNA in question must be much longer than 150 base pairs.
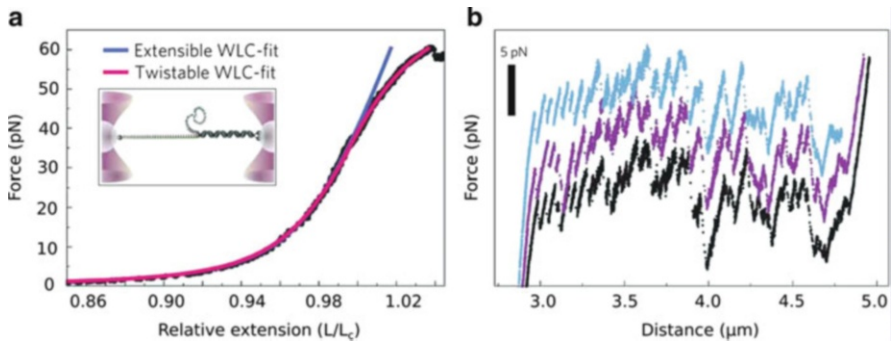
Fig. 2.3 Twistable worm-like chain and sawtooth pattern during the overstretching transition. (**a**) tWLC model versus data. The experimental values of pulling force versus molecular extension (*black*) are compared to the extensible worm-like chain model (*blue*) and the twistable worm-like chain model (*pink*). *Inset*: pulling geometry. The dsDNA is attached to bead handles at three sites. (**b**) Sawtooth unfolding pattern at the 65 pN overstretch plateau during three different pulls, see Sect. 2.3.3. The dsDNA is attached as in the *inset* of (**a**) so that only one strand has a free end. Figures from Gross et al. (2011)

For single-stranded RNA and DNA, on the other hand, the minimum length for applying the WLC models is equivalent to less than ten nucleotides.

2.3.3   DNA Unzipping

Early single-molecule DNA investigations showed that a sequence-dependent sawtooth pattern occurs in the force–extension curve when a long piece of dsDNA is unzipped by a force perpendicular to the helix (Essevaz-Roulet et al. 1997). Unzipping occurs at forces of about 10–15 pN, much lower than the forces required for overstretching when dsDNA is pulled along the length of the helix. The peaks in the unzipping sawtooth pattern are correlated with GC-rich areas in the dsDNA because GC base pairs are stronger than AT base pairs, requiring more force to open. Thus, researchers found that dsDNA unzipping occurs in bursts at high speed in AT-rich regions and lower speed in the GC-rich regions.

Sawtooth patterns are also observed during overstretching when force is applied parallel to the helical direction, supporting the hypothesis described in the previous section (Sect. 2.3.1) that the overstretching plateau represents base pairs melting. Recent experiments by Gross et al. (2011) further corroborate this explanation by showing that the sawtooth patterns observed during overstretching at room temperature and low salt concentration (50 mM NaCl) are reproducible and sequence correlated just like those seen in unzipping experiments (Fig. 2.3b). This reproducible slip-stick behavior of melting dsDNA is most clearly visible in experiments when only a single end of the tethered dsDNA is free; hence, the melting into ssDNA will initiate from this point only, as in the inset in Fig. 2.3a.

2.3.4   DNA Twist

The twist-stretch coupling function $g(F)$ was first quantified by monitoring the torque on the DNA together with the change in length of the molecule using magnetic torque tweezers (Gore et al. 2006). Remarkably, DNA at first overwinds when stretched: the helix winds more closely as the molecule is lengthened, conserving volume. If pulled by forces stronger than 30 pN, the DNA eventually does unwind as it lengthens further.

Conversely, if the dsDNA is overwound by torque, it stretches. Twisting the molecule, one complete rotation causes it to lengthen by approximately 0.5 nm. This lengthening continues until eventually, with increased winding at constant force, the DNA shortens as might be expected because supercoiling is induced in the double-stranded structure (Gore et al. 2006).

Generally, if dsDNA is strongly over- or underwound at low force, it forms writhes and plectonemes (supercoils), resulting in shorter molecular extension (Strick et al. 1998). An overview of the research on the transitions that DNA undergoes when over- or underwound has been laid out by Bryant et al. (2012).

2.3.5   Higher-Order DNA Structure

The packaging of DNA in chromatin is a major topic of single-molecule research, recently reviewed by Killian et al. (2012). Chromatin is a higher-order DNA structure composed of dsDNA wrapped around histone proteins in tight bundles called nucleosomes. Force spectroscopy techniques have been used to probe how dsDNA is bound to individual histones, how nucleosomes are distributed along the DNA, and how series of nucleosomes are arranged in relation to each other in the chromatin fiber.

An example of such a study is the use of magnetic tweezers by Kruithof et al. (2009) to deduce the folding geometry of nucleosome-bound DNA in chromatin. The group calibrated the magnitude of the force applied by the magnetic tweezers at different heights relative to the sample chamber and were therefore able to measure the response of the chromatin at different forces. They used this ability to investigate the force response of two different types of chromatin fibers. Both types of fibers were previously known to wrap into a structure with a diameter of about 30 nm, but the spatial arrangement of the nucleosomes within the fibers was debated. One type of fiber had a nucleosome repeat length of 197 base pairs; the other had a nucleosome repeat length of 167 base pairs. The nucleosome repeat length is the number of base pairs per nucleosome, some of which is DNA is wrapped around the histone complex and some of which may constitute linker DNA between the histones. In nature a variety of different repeat lengths are found. A repeat length of 197 base pairs allows for an average amount of linker DNA, while 167 base pairs allow for no linker DNA at all. How could these two types of fiber wrap into apparently similar structures?

To investigate this, chromatin fibers were attached between the chamber surface and a magnetic bead and stretched. The results showed that both types of chromatin fiber stretch gradually up to a force of about 4–6 pN. Above this force, the force–extension curve displays a plateau, which the group attributed to the disruption of nucleosome–nucleosome interactions, i.e., dissociation of the fiber.

Focusing on the slope of the curve before the nucleosome dissociation plateau, the group was able to show that the chromatin fibers behaved like Hookean springs and that fibers with normal-length linker DNA had lower stiffness and were shorter than fibers lacking linker DNA. This led the group to conclude that with normal-length linkers, chromatin forms a single-helix coil, while without linkers it forms a stacked zigzag coil. The softer of the two types of coil will stretch and contract more with thermal fluctuations than the stiffer type of fiber, possibly allowing for different types of interactions with chromatin-modifying proteins. The group expects that both types of structure and possibly others will occur naturally (Kruithof et al. 2009).

2.4   Kinetics

Molecular force spectroscopy is often used to investigate structural changes from one molecular state to another, e.g., the opening and closing of DNA or RNA hairpins. As such experiments inevitably involve a force acting on the molecule of interest, traditional equilibrium thermodynamics is inadequate to describe the process. Recent advances in nonequilibrium thermodynamics are, however, providing tools to extract thermodynamic constants from nonequilibrium experiments. The following section describes a theoretical framework that can be used to find the kinetic transition rates and the brittleness of the investigated molecule. In Sect. 2.5, we outline recently discovered thermodynamic principles that allow quantification of the Gibbs free energy change from nonequilibrium data and give access to the profile of the energy landscape.

2.4.1   Rate of Transition and Molecular Brittleness

Investigating molecular structure with optical or magnetic tweezers by applying either a constantly increasing force (force ramp) or a constant force to a single molecule usually results in data series of transition forces or waiting times, respectively. Both types of experiments measure the change in extension of the molecule due to a structural transition. From the distribution of forces or waiting times, information may be extracted about the rate of opening at different forces, $k(F)$, with the rate of opening at zero force, k_0, especially of interest. From the change in extension, the number of base pairs or single nucleotides involved in the transition may be calculated, see Fig. 2.4b for an example.
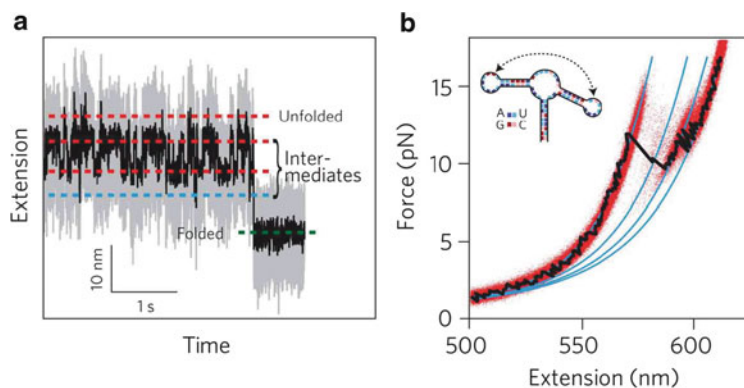
Fig. 2.4 Data from unfolding a riboswitch aptamer (more details on the experiment are given in Sect. 2.5.2): (**a**) Constant-force OT data. The aptamer hops between unfolded, folded, and intermediate states with different molecular extensions. (**b**) 700 overlaid force–extension curves from OT force-ramp experiments (data *red*, average *black*). Intermediate states corresponding to different (*blue*) equilibrium WLC stretch curves are evident. *Inset*: expected closed state of the aptamer. The *arrow* indicates expected interaction between the two hairpin loops. Reproduced with permission from Gupta et al. (2011)

Nanopore experiments for investigating molecular structure do not directly yield force or distance measurements. However, the series of waiting times between molecule insertion and molecule passage through the membrane likewise yield the rate of reaction.

Data on changes in extension may be used to identify intermediate states. In constant-force experiments, several distinct equilibrium molecular lengths corresponding to different molecular states may be directly observed (Fig. 2.4a). Similarly, in force-ramp experiments, it may be clear that the molecule is passing between several equilibrium force–extension curves. In this case intermediate states are most clearly seen by aligning many curves of force versus molecular extension (Fig. 2.4b). Curves corresponding to different molecular states may be distinguished by fitting to extension curves for folded, intermediate, or unfolded configurations. The curves are modeled by using the appropriate stretching model for the force regime being probed, i.e., the worm-like chain model or the twistable worm-like chain model, as described in Sect. 2.3. When a sudden change in molecular extension occurs, the unfolding/refolding length may be related to the number of nucleotides being exposed/folded away using the same theory.

Since the most commonly applied kinetic theories are valid only for two-state transitions, intermediate states should in principle be identified from the raw data before the kinetic analysis. Assuming that different types of transitions can be separated into distributions, the waiting times or transition force data for each sub-transition are then usually analyzed separately.
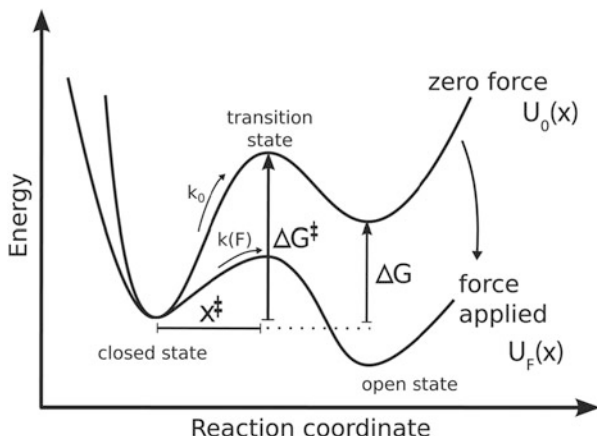
Fig. 2.5 Generic energy landscape profile along an arbitrary reaction coordinate for a two-state system with an open and a closed state separated by an energy barrier. The barrier is characterized by $x^{\ddagger}$, the distance from the closed state to the transition state, and $\Delta G^{\ddagger}$, the energy of activation along the reaction coordinate. ΔG is the Gibbs free energy change of the transition, which is independent of the reaction coordinate. k_0 and $k(F)$ are the rates of reaction at zero force and force F, respectively. The energy surface, $U_0(x)$, is in effect tilted by the potential energy added by the application of force, turning it into an energy surface $U_F(x)$. During a typical pulling experiment, the reaction coordinate, x, corresponds to, e.g., the position of the optical trap or the extension of the molecule. Figure inspired by Dudko et al. (2006)

For a simple two-state transition, several models exist for finding $k(F)$ from the distribution of unfolding forces. The most common approach is based on Bell's formula (Bell 1978):

$$k(F) = k_0 e^{Fx^{\ddagger}/(k_B T)} \tag{2.3}$$

Here, k_B is the Boltzmann constant and T the temperature as before, while $x^{\ddagger}$ is a quantity called the "distance to the transition state," which is a "distance" in the energy landscape of the molecule between a closed state and the energy barrier to an open state. The transition state is located at the top of the energy barrier. If $x^{\ddagger}$ is measured along a coordinate of molecular extension (or the coordinate of trap position), $Fx^{\ddagger}$ is the energy required for the molecule to reach the transition state. Bell's formula is thus very similar to the Arrhenius equation, which is obtained by replacing $Fx^{\ddagger}$ by E in Eq. (2.3).

Figure 2.5 illustrates an energy landscape with a certain distance, $x^{\ddagger}$, to the transition state. Here, the profile of an energy landscape surface at zero force, $U_0(x)$, varies along an arbitrary reaction coordinate, and the distance to the transition state, $x^{\ddagger}$, is simply a distance along this virtual coordinate between the original (closed) state and the transition state. Similarly, the energy of activation, $\Delta G^{\ddagger}$, quantifies the energy difference between the closed and transition states at zero force. Like the

zero-force rate of transition, k_0, the values of $x^{\ddagger}$ and $\Delta G^{\ddagger}$ depend on the reaction coordinate along which the energy profile is drawn (Dudko et al. 2008).

When the reaction coordinate is the molecular extension, $x^{\ddagger}$ is a useful measure of the brittleness of the molecule: it directly shows how much the molecule can be deformed before it switches from one state to another. A small value of $x^{\ddagger}$ indicates a brittle molecule, while a larger value indicates a more compliant one. An example of a reaction wherein molecular extension is directly correlated to molecular state is the unzipping of a DNA or RNA hairpin. Simple RNA and DNA hairpins have generally been found to be less brittle than complex structures such as RNA pseudoknots (see Sect. 2.5.3). For DNA hairpins, $x^{\ddagger}$ has been found in the range of 2–20 nm (Woodside et al. 2006), increasing with the length of the hairpin stem. A simple RNA hairpin and an RNA hairpin with a side branch likewise had $x^{\ddagger}$ of about 12 nm, while a more complex RNA hairpin structure stabilized by magnesium ions had $x^{\ddagger}$ of only 1.6 nm (Liphardt et al. 2001). For RNA pseudoknots, values of $x^{\ddagger}$ have been found as low as 0.2 nm (Hansen et al. 2007).

2.4.2 Extension and Molecular States

When DNA or RNA hairpins are unzipped, the transition generally takes place in a single clear "hop" in the extension-time series of a constant-force experiment (Fig. 2.4a) or a clear "rip" in the force extension curve derived from a force-ramp experiment (Fig. 2.4b). During each rip or hop, base pairs are opened in quick succession from the base of the helix to yield a fully unfolded structure. For this type of reaction, $x^{\ddagger}$ truly corresponds to a change in the end-to-end extension of the molecule, corresponding to a number of opened base pairs. Since $x^{\ddagger}$ measures the distance between the closed state and the energy barrier, the physical location of the energy barrier can be found by translating $x^{\ddagger}$ into base pair length, taking into account the stretching of the molecule at the transition force by using the theory described in Sect. 2.3 (Woodside et al. 2006).

However, an intrinsic problem with looking at energy landscapes along the coordinate of molecular extension is that in some cases, several different molecular states might be associated with a single molecular extension. This occurs if other thermodynamic variables are more important for determining the state of the molecule than its extension. In such cases the folding pathway of the molecule might not scale linearly with molecular extension in the way that polynucleic acid hairpin unwinding does, and application of force may in fact make a molecular transition less likely to occur (Dudko et al. 2008). This might be the case, e.g., for a polynucleic acid wound around itself or around another molecule: pulling may tighten the winding, making a transition to the open state less likely, at least up to a certain force level.

2.4.3 Kinetic Parameters from Force Data

For force-ramp experiments, where the force is increased over time at a constant loading rate, r, an expression may be derived from Eq. (2.3) for k_0 and $x^{\ddagger}$ in terms of the probability, P, that the molecule has not yet undergone a transition. In the derivation it is assumed that the transition is a first-order two-state reaction, so that the survival probability of the initial molecular state is an exponential function of time. This assumption requires that the force is increased slowly enough for the transition rate to depend directly on the force, i.e., a quasi-adiabatic transition (Dudko et al. 2008). The expression is (Hummer and Szabo 2003)

$$r \ln P = -\frac{k_0 k_B T}{x^{\ddagger}} \left(e^{F x^{\ddagger}/(k_B T)} - 1 \right) \tag{2.4}$$

With this expression, using the known loading rate and the empirical probability distribution of transition forces, one can plot $r \ln P$ against F (the forces at which molecular transitions are observed) and fit Eq. (2.4) to the data to obtain estimates of k_0 and $x^{\ddagger}$. Note that $p(F)$ depends on r, so that the average unfolding force increases with the loading rate (Dudko et al. 2010).

For constant-force experiments, finding k_0 and $x^{\ddagger}$ requires finding the transition frequency (i.e., the inverse of the average waiting times between transitions) for a range of forces. A fit is then made directly to Bell's formula [Eq. (2.3)] to find the parameters k_0 and $x^{\ddagger}$, as done, e.g., in the classical study of RNA hairpins by Liphardt et al. (2001).

2.4.4 Expanded Kinetic Theory

Although the approach presented in Sect. 2.4 above is useful, its assumptions are unlikely to be true in single-molecule experiments. In recent theoretical work, Dudko, Hummer, and Szabo (2006) have incorporated a more accurate assumption about the energy landscape: as the force increases, the whole "energy landscape" of the structure changes, including $x^{\ddagger}$, as illustrated in Fig. 2.5. To allow for this, the researchers explicitly introduce a theoretical free energy surface $U_F(x)$ along the pulling coordinate x:

$$U_F(x) = U_0(x) - Fx,$$

where $U_0(x)$ is the free energy surface at zero force expressed by one of several simple geometric formulas and Fx is the potential applied by pulling the molecule along the coordinate x. Two possible shapes of $U_0(x)$ are shown in Fig. 2.6: cusp shaped and linear cubic. The cusp shape derives from a parabolic function with a vertical drop-off beyond the energy barrier at $x^{\ddagger}$, while the linear-cubic shape is a
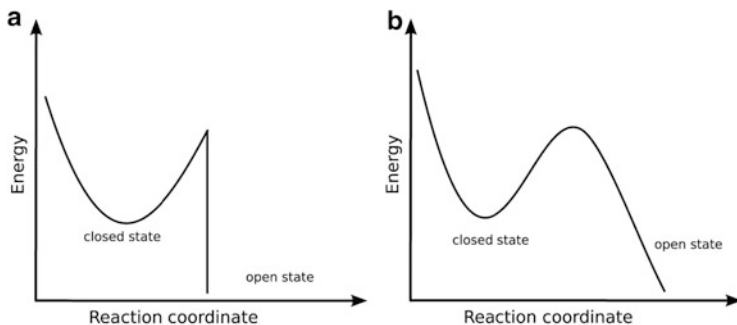
Fig. 2.6 Free energy surfaces $U_0(x)$ at zero force: (**a**) Cusp-shaped energy landscape consisting of a parabolic function with a vertical drop-off beyond the energy barrier at $x^{\ddagger}$. (**b**) Linear-cubic energy landscape consisting of a cubic function with an asymptotically linear drop-off beyond the energy barrier. Energy profile functions are defined in Dudko et al. (2006)

cubic function with a valley at the initial state and an asymptotically linear drop-off beyond the energy barrier.

Assuming that $U_0(x)$ is shaped like one of the two functions shown in Fig. 2.6, an analytical expression can be found for the transition rate, $k(F)$, at force F (Dudko et al. 2006):

$$k(F) = k_0 \left(1 - \frac{\upsilon F x^{\ddagger}}{\Delta G^{\ddagger}}\right)^{1/(\upsilon-1)} e^{\Delta G^{\ddagger}\left[1-(1-\upsilon F x^{\ddagger}/\Delta G^{\ddagger})^{1/\upsilon}\right]} \tag{2.5}$$

where $\Delta G^{\ddagger}$ as above is the apparent energy of activation and υ is a parameter describing U_0. Setting $\upsilon = 1/2$ corresponds to the cusp-shaped U_0 energy landscape, $\upsilon = 2/3$ corresponds to the linear cubic. Both shapes imply that there is no return across the energy barrier once the molecule has passed $x^{\ddagger}$. This closely resembles the assumption of a first-order transition made to derive Eq. (2.4). Indeed, setting $\upsilon = 1$, Eq. (2.5) reduces to Eq. (2.4). To find k_0, $x^{\ddagger}$, and $\Delta G^{\ddagger}$, Eq. (2.5) can be fitted to empirical values for $k(F)$ (constant-force experiments) or to values of $k(F)$ calculated from an empirical estimate of $p(F)$, the probability distribution for transition at different forces (force-ramp experiments) (Dudko et al. 2008).

Because there are three unknowns in the fit and because a pooling of data is needed to empirically estimate $k(F)$ over a range of forces, a large number of data points are needed. Nonetheless, Dudko et al. (2007) have successfully applied the theory to experimental data for unzipping of DNA hairpins using nanopore force spectroscopy as outlined in Sect. 2.2.3. One advantage of this method is that it makes more accurate assumptions than Bell's formula about the distance to the transition state for high force transitions.

2.5 Nonequilibrium Thermodynamics

Within the last 15 years, new thermodynamics theories have enabled the derivation of the Gibbs free energy change, ΔG, from nonequilibrium nanoscale experiments. The relation first discovered is the Jarzynski equality (JE) (Jarzynski 1997), which links the work spent to drive a system from an initial to a final state to the Gibbs free energy difference between the two states:

$$\overline{\exp\left(-\frac{W_i}{k_{\mathrm{B}}T}\right)} = \exp\left(-\frac{\Delta G}{k_{\mathrm{B}}T}\right) \tag{2.6}$$

Here W_i is the work measured for either a forward or a reverse transition (e.g., either the work required to open a DNA hairpin or the work gained when it reanneals). Note that the left-hand side of Eq. (2.6) is an average over many measurements of the transition work, W_i. The equality requires that the transition being measured, whether forward or reverse, begins and ends in thermodynamic equilibrium.

The second relation is the Crooks Fluctuation Theorem (CFT). The Jarzynski equality, presented 2 years before the CFT, may easily be derived from the CFT. The CFT states (Crooks 1999; Collin et al. 2005)

$$\frac{P_{\mathrm{F}}(W)}{P_{\mathrm{R}}(-W)} = \mathrm{e}^{(W-\Delta G)/k_{\mathrm{B}}T} \tag{2.7}$$

where W is the amount of work done on the construct, $P_{\mathrm{F}}(W)$ is the probability of the amount of work W being exerted by the system on the construct during the forward transition, $P_{\mathrm{R}}(-W)$ is the probability of the amount of work W being absorbed by the system during the reverse transition, and ΔG as above is the reversible change in the Gibbs free energy of the construct between the initial and the final state.

The CFT applies under the following assumptions:

- The state in which the forward transition begins must be the same as the state in which the reverse transition ends and vice versa.
- The transition, though overall irreversible, must be microscopically reversible: At any moment, if the velocity were reversed, the system would be just as likely to move in the reverse direction as it was to move in the forward direction with the original velocity.

The latter condition means that at any given moment, the forward reaction is indistinguishable from the reverse reaction. This is true even though overall, when looking at many irreversible forward and backward reactions, there is hysteresis in the system as in Fig. 2.7, i.e., the forward and reverse reactions on average require and return different amounts of energy.
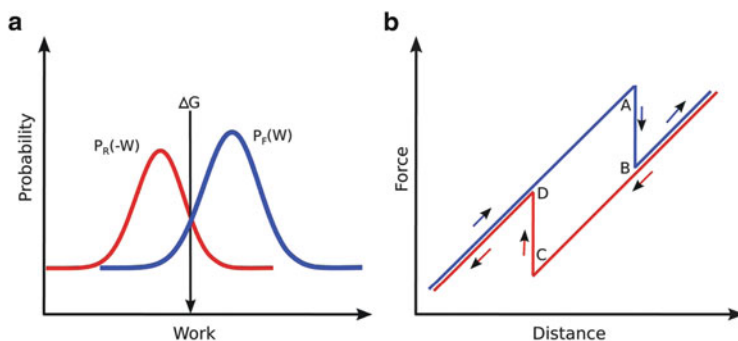
Fig. 2.7 Illustration of the Crooks fluctuation theorem. (**a**) The Crooks fluctuation theorem states that the Gibbs free energy change, ΔG, of an irreversible transition is equal to the work value where the forward and reverse transition work distributions intersect. The work distributions need not be Gaussian distributions. (**b**) Irreversible transition during a force-ramp molecule pulling experiment. The model curve shows force versus distance moved by the system (e.g., the optical trap, magnetic tweezers, or sample chamber). *Blue*: forward reaction. *Red*: reverse reaction. The transition takes place during the zip from A to B and the zip from C to D. The area under the *curve* in the direction of the *arrows* corresponds to the work performed on the system

The CFT implies immediately from Eq. (2.7) that at the point where $P_F(W) = P_R(-W)$, $W = \Delta G$, as shown in Fig. 2.7a. Thus, even though the reaction is irreversible, ΔG for the reversible transition can be found directly from the intersection of the empirical probability distributions of work for the forward and reverse transitions. Note that $P_F(W)$ and $P_R(-W)$ are not always Gaussian, although they may often be approximated by Gaussian curves when the transition is close to equilibrium. If the transition were reversible, $P_F(W)$ and $P_R(-W)$ would overlap and both center on ΔG. The further the reaction is from equilibrium, the more heat is dissipated and the less $P_F(W)$ and $P_R(-W)$ overlap, making it more difficult to find their intersection. However, using Bennett's acceptance ratio, it can still be done (Collin et al. 2005).

Compared to the CFT, the Jarzynski equality has the advantage that it requires data for transitions only in one direction. The disadvantage, which is quite substantial, is that since it averages exponential functions, the smallest work values influence the result the most. Very large numbers of measurements are required to give good statistics, and the further the process is from equilibrium, the more data are required. In practice, Jarzynski noted, it would probably be very hard to obtain enough data if the heat dissipation is more than about $k_B T$ (Jarzynski 1997). Ritort et al. (2002) have calculated that if the dissipation is more than about 5 $k_B T$, more than 1,000 experimental repetitions are needed. However, a better estimate may be obtained if the Jarzynski equality is used on both unfolding and refolding work distributions and the two are averaged, as done by Collin et al. (2005).

2.5.1 Work Measurement in Practice

To apply the JE and CFT, the work is generally calculated from the force applied to the system times the distance moved by the system. For single-trap optical tweezers experiments, this should be done by integrating the force along the axis of the distance moved by the instrument, i.e., the area under the curve in Fig. 2.7b. The distance moved by the system is the distance moved by the trap, the sample chamber surface, or a bead held in a pipette (Mossa et al. 2009). For experiments where the instrument controls force rather than distance (e.g., magnetic tweezers experiments), molecular extension should be integrated along the force axis.

Integration of the force along distance moved by the instrument is usually not equivalent to integration along the axis of molecular extension because molecular extension fluctuates, e.g., with the movement of the bead in the trap. However, the error from integrating along the axis of molecular extension is reduced to essentially nothing if the data are sufficiently smoothed. Mossa et al. (2009) find that the error in ΔG calculated with the CFT can be up to about 10 % if the area under the force–extension curve is used as the work rather than the area under the force–distance curve. Conversely, the correctly calculated ΔG (using the work under the force–distance curve in the CFT) necessarily contains a contribution from the bead movement in the trap, which should be subtracted if the aim is to find ΔG for the molecule only (Mossa et al. 2009). Finding this correction requires data with very low noise, which necessitates very short molecular handles and a very well-aligned system where the force on the molecule can be measured with extremely high precision (Alemany et al. 2012). Work derived as the area under the force–extension curve requires no such correction and as mentioned above may yield reasonable results when the data are smoothed.

In either case, to apply the CFT, the integral of each experimental force–distance or force–extension curve is calculated between a starting force corresponding to the lowest transition force observed and an ending force corresponding to the highest transition force observed (Collin et al. 2005). For the JE, the entire curve should be integrated, as the transition must start and end in equilibrium.

Apart from contributions from bead movement, the work found from integrating the force–distance or force–extension curve for a pulling experiment also often contains a substantial component from stretching the DNA or RNA under investigation. Applying the JE or the CFT to this work results in a ΔG value that includes the change in internal energy required for pure stretching. If the aim is to find ΔG for only a transition between distinct chemical states (e.g., hairpin unzipping), the work used to stretch the structure and any handles must be subtracted. This is done by calculating the theoretical value of the stretching work using the appropriate stretch model for the type of polymer and the force regime in question (see Sect. 2.3). The assumption is that the model describes the stretching well and that the stretch and relax are reversible on the timescales of the experiment. When both double- and single-stranded polynucleic acids are involved, the contribution from stretching each of these types of polymer is added in sequence (Collin et al. 2005).
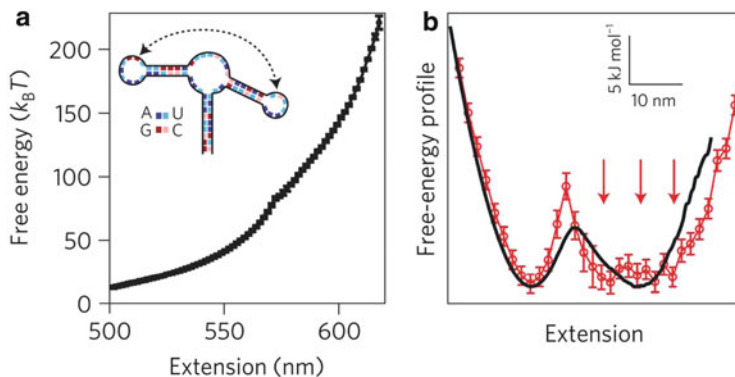
Fig. 2.8 Mapping the energy landscape of a riboswitch aptamer (data samples shown in Fig. 2.4): (**a**) Zero-force energy profile of the aptamer calculated from nonequilibrium experimental data. *Inset*: expected closed state of the molecule, also shown in Fig. 2.4b. The *arrow* shows expected interaction between the two hairpin loops. (**b**) Energy profile tilted by a force so that the closed and open states are approximately in equilibrium. *Black*: profile calculated from equilibrium (constant-force) measurements. *Red*: profile calculated from nonequilibrium (force-ramp) measurements. *Arrows*: possible intermediate states. Reproduced with permission from Gupta et al. (2011)

Note that the method is vulnerable to error arising from the estimate of the stretch contribution, especially for structures being unfolded far from equilibrium, since the stretch correction is larger in that case. The error also increases for small structures, since the WLC stretching models assume $L_c \gg L_p$.

2.5.2 Intermediate States in the Energy Landscape

Since the Jarzynski equality requires only that the system being measured starts or ends in equilibrium, it can be used to calculate the energy required to reach any nonequilibrium state. This means that the JE can be used to map the full energy landscape profile of a nonequilibrium transition, as originally suggested by Hummer and Szabo (2001). For pulling experiments, the mapping immediately yields the energy profile along the coordinate of pulling distance, but it can be transformed into a profile along the coordinate of molecular extension using several different methods (Hummer and Szabo 2010). To exploit the full data set when data for both forward and reverse transitions are available, energy profile mapping can also be done using the CFT; one method has been presented by Minh and Adib (2008).

The Hummer–Szabo method was first applied to RNA hairpin data by Liphardt et al. (2002) in their demonstration of the validity of the Jarzynski equality. Recently, Gupta et al. (2011) used the same principle to find the energy landscape profile of a DNA hairpin and an RNA riboswitch aptamer from force-ramp experiments. Figure 2.8 shows the experimental energy landscape profiles calculated for the riboswitch. The group employed optical tweezers in a geometry much

like the one shown in Fig. 2.1a. From constant-force and force-ramp data, they had seen that intermediate states existed in the energy landscape (data shown in Fig. 2.4). Figure 2.8a displays the calculated energy profile at zero force, illustrating how similar the intermediate states are in potential energy: they are not even visible as bumps in the energy profile along the coordinate of molecular extension. Figure 2.8b shows the energy profile when the aptamer is held at constant force near equilibrium between the open and closed states. The arrows in the figure indicate that at least three different states may be reached once the main energy barrier between the closed and the open state is passed. Comparing Figs. 2.8a and 2.8b, it becomes clear how the application of force tilts the energy landscape so that states that are highly unfavorable at zero force become favorable.

One main achievement of Gupta et al. (2011) is that the group was able to validate their nonequilibrium energy profile against an energy profile calculated with a more data-intensive approach involving equilibrium measurements. Gupta et al. (2011) found that the nonequilibrium approach yielded more information about intermediate states. The black curve in Fig. 2.8b shows the energy profile reconstruction from equilibrium data, which does not show any intermediate states. In contrast, the red curve from the nonequilibrium data does hint at possible intermediate states (arrows).

Note that the energy landscapes in Fig. 2.8 include the free energy used to stretch the dsDNA handles attached to the RNA riboswitch aptamer. To find the energy landscape of the aptamer, the free energies of the aptamer and the handles can be deconvolved; this was done by Woodside et al. (2006) in calculations of the equilibrium energy landscape of DNA hairpin unfolding. Hummer and Szabo (2010) suggest that alternatively one may approximate the handles as harmonic springs whose energy can be subtracted if their stiffness can be estimated.

Building on these advances, a thermodynamic approach developed by Junier et al. (2009) directly addresses the possibility that the molecule may be in many different states during experiment. This Expanded Fluctuation Theorem builds on the CFT by allowing calculation of transition energies even when the initial and final states of the molecule in a series of pulling experiment are not always the same, but rather represent a range of possible states including intermediates. The Expanded Fluctuation Theorem has recently been applied to data for DNA hairpin unfolding to reveal the energy of formation of a variety of intermediate states (Alemany et al. 2012). A prerequisite for the application of the theorem is a subtle determination of the populations of molecules corresponding to different intermediate states. This requires very low noise data, in the case of Alemany et al. (2012) attained using constructs with extremely short handles.

2.5.3 mRNA Pseudoknot Kinetics

Messenger RNA (mRNA) pseudoknots are secondary structures on mRNA that influence protein synthesis through their ability to sometimes shift the ribosomal
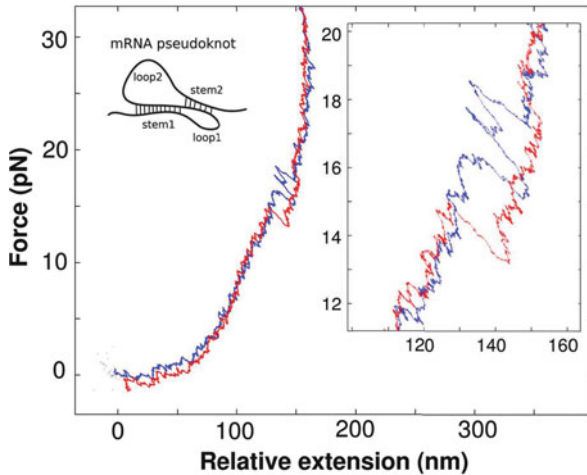
Fig. 2.9 Force versus molecular extension for an mRNA sequence containing a pseudoknot. Pulling experiment with two optical traps; the single-stranded mRNA containing the pseudoknot sequence was hybridized to DNA handles linked to polystyrene beads in the traps by biotin–streptavidin and digoxigenin–antidigoxigenin bonds. *Blue*: moving the beads apart, extending the molecule. *Red*: relaxing. *Left inset*: schematic structure of an mRNA pseudoknot. *Right inset*: zoom of the region in which the unfolding and refolding transitions take place

reading frame (see general pseudoknot structure in Fig. 2.9, left inset). This means that two different proteins can be produced from a single mRNA sequence, one frameshifted, one not. How efficient a given pseudoknot is at inducing frameshift may depend on sequence-correlated structural characteristics, but how exactly sequence relates to 3-D structure and to frameshifting is currently unclear. Several attempts to uncover the relationship between frameshift efficiency and mechanical properties have been made using optical tweezers; yet controversy remains in the literature regarding the deciding factors for pseudoknot strength (Ritchie et al. 2012). Nonetheless, mechanical strength and frameshift efficiency may be correlated at least within certain regimes and pseudoknot families (Hansen et al. 2007; Chen et al. 2009).

In contrast to experimental unfolding and refolding of hairpins, where opening and closing transitions generally happen in single clear steps, pseudoknot unfolding traces often display several unfolding or refolding steps of various sizes, which are clear indications of intermediate states (Fig. 2.9). A focus of pseudoknot investigations has therefore been the elucidation of intermediate steps and possible folding pathways for the mRNA sequence. OT investigations of mRNA pseudoknots have usually been force-ramp experiments, where the molecule is pulled at a constant rate, revealing how much force is needed to open the molecular structure and at which force it re-forms. Figure 2.9 shows a typical force–extension curve for an mRNA molecule expected to form a pseudoknot. Clear unfolding and

refolding events are observed, including unfolding and refolding to an intermediate state around 18 pN.

A pseudoknot usually consists of two loops and two stems that are interlinked. The steps observed in unfolding transitions may therefore correspond either to the full pseudoknot unfolding into single-stranded mRNA or to a single loop and stem opening, forming an intermediate structure. As described in Sect. 2.4.1, the length that the structure unfolds or refolds is a signature of how many base pairs are opened or closed during a transition, indicating which structural transition takes place. In Fig. 2.9, the largest transition steps are about 13–16 nm, but the expected unfolding length of the pseudoknot at these forces is expected to be at least 25 nm. Thus, the steps in the figure may all represent transitions to or from an intermediate state. For instance, it may be that the structure being opened is not a pseudoknot but a hairpin-like formation made up of one stem and one loop of the predicted pseudoknot, an explanation which corresponds well to the relatively low force observed for the transitions. In the presence of magnesium ions (as in the experiment shown in Fig. 2.9), pseudoknots often unfold at forces in the range of 20–50 pN.

Like hairpin investigations, pulling experiments with pseudoknots have been used to investigate the brittleness and the energy of formation of the structures observed using the theory described in Sects. 2.4 and 2.5. Frameshift-inducing pseudoknots are often strong, brittle structures, but the sequences capable of forming such pseudoknots also often form intermediate, weaker, and more pliable structures (Chen et al. 2009); as described, this may be the case in Fig. 2.9. Such intermediates may interfere less with the translating ribosomes, offering a possible reason why frameshifting does not always occur.

2.6   Summary and Outlook

Force spectroscopy has opened up a multifaceted toolbox for investigating the response of DNA and RNA to mechanical perturbation. Optical and magnetic tweezers, nanopore force spectroscopy, and combinations hereof, sometimes integrated with fluorescence measurements or the application of flow, allow researchers to stretch, twist, unzip, or relax single molecules, quantifying their direct response to force. The aim is often to understand the response of polynucleic acids to physiological or artificial conditions such as temperature, buffer, reactants, or mechanical strain. Induction of changes in conformation allows identification of intermediate states and calculation of energies of formation and transition rates.

This chapter describes the typical methods and fundamental areas of research in DNA and RNA force spectroscopy. The research areas include model description and understanding of the twist and stretch of double-stranded DNA, as well as analysis of energy changes, kinetic rates, and other energy landscape features characterizing force-induced structural changes in RNA and DNA.

Outside of the subjects covered here, a large field of research employs force spectroscopy to examine the interactions of polynucleic acids with transcription and translation factors, with histones and nucleosomes, with the enzymatic machinery of the cell, and with other DNA- and RNA-modifying proteins. This field is constantly growing, and in the coming years we may expect investigations not only of the effect of single polynucleic acid modifying ligands and molecular motors, e.g., a single ribosome moving on a piece of mRNA, but also of the collective action of several molecular motors and/or polynucleic acid modifying ligands. Already, the compound action of two RNA polymerases has been followed in vitro (Jin et al. 2010).

Another frontier is in vivo testing of DNA and RNA response to mechanical manipulation. Optical and magnetic tweezers are both able to act upon objects within living cells, and in vivo experiments have already been carried out to measure the action of molecular motors such as kinesins, which take part in chromosome segregation during cell division. Though challenges remain in how to internalize probe beads into cells and ensure specific single-molecule attachment, polynucleic acids and their associated molecular machinery may soon be measured in their native biological environment (Oddershede 2012). Alongside such in vivo experiments, in vitro research will continue to explore the effects of buffer, temperature, and other environmental factors on DNA and RNA structure and transitions.

To assist investigations, continued improvement of technical capabilities may be expected in coming years, allowing trapping of smaller items, application of higher force, measurements with higher precision, and more widespread mixing of techniques. Combinations of optical and magnetic tweezers (Crut et al. 2007), optical tweezers and nanopores (Keyser et al. 2006), and fluorescence in conjunction with either OT, MT, or NFS (van Mameren et al. 2009; Gore et al. 2006; McNally et al. 2010) have already been demonstrated. Some fluorescent molecules are even able to act directly as probes of force or distance; these properties are used, e.g., in fluorescence resonance energy transfer (FRET) measurements (Iwai and Uyeda 2008; Chen et al. 2012).

Rapid theoretical development is also taking place. In coming years we may thus better understand how kinetic data from force spectroscopy experiments can illuminate the entire energy landscape of the molecule. Molecules being altered by enzymes or undergoing structural transformations due to temperature or pressure fluctuations may pass along entirely different energy landscape profiles than the same molecule when exposed to tension along a single dimension. Yet Dudko et al. (2011) have already shown that under certain conditions, kinetic data obtained from force spectroscopy experiments provide general information about the underlying molecular energy landscape.

Additionally, we expect continued refinement of data processing for all force spectroscopy techniques, e.g., in eliminating handle effects for optical and magnetic tweezers results and accounting for nanopore interaction with polynucleic acid sequence. Methodological advances may also allow simpler elucidation of

intermediate states from limited data and from experiments where the molecules may not all start out in the same state.

In conclusion, force spectroscopy has already provided detailed knowledge on the properties of double- and single-stranded DNA, of the strength and force response of DNA and RNA hairpins, and of the folding of more complex structures. In coming years, probing of DNA, RNA, and associated molecules by force will continue to provide new insights into the core mechanisms of molecular biology.

References

Alemany A, Mossa A, Junier I, Ritort F (2012) Experimental free-energy measurements of kinetic molecular states using fluctuation theorems. Nat Phys 8:688–694

Bell GI (1978) Models for the specific adhesion of cells to cells. Science 200(4342):618–627

Bizarro CV, Alemany A, Ritort F (2012) Non-specific binding of Na^+ and Mg^{2+} to RNA determined by force spectroscopy methods. Nucleic Acids Res 40(14):6922–6935

Boal DH (2002) Mechanics of the cell. Cambridge University Press, Cambridge

Bryant Z, Oberstrass FC, Basu A (2012) Recent developments in single-molecule DNA mechanics. Curr Opin Struct Biol 22(3):304–312

Bustamante C, Marko JF, Siggia ED, Smith SB (1994) Entropic elasticity of λ-phage DNA. Science 265(5178):1599–1600

Bustamante C, Macosko JC, Wuite GJL (2000) Grabbing the cat by the tail: manipulating molecules one by one. Nat Rev Mol Cell Biol 1(2):130–136

Chen G, Chang K, Chou M, Bustamante C, Tinoco I Jr (2009) Triplex structures in an RNA pseudoknot enhance mechanical stability and increase efficiency of -1 ribosomal frameshifting. Proc Natl Acad Sci USA 106(31):12706–12711

Chen H, Meisburger SP, Pabit SA, Sutton JL, Webb WW, Pollack L (2012) Ionic strength-dependent persistence lengths of single-stranded RNA and DNA. Proc Natl Acad Sci USA 109(3):799–804

Cluzel P, Lebrun A, Heller C, Lavery R, Viovy J, Chatenay D, Caron F (1996) DNA: an extensible molecule. Science 271(5250):792–794

Collin D, Ritort F, Jarzynski C, Smith SB, Tinoco I Jr, Bustamante C (2005) Verification of the Crooks fluctuation theorem and recovery of RNA folding free energies. Nature 437:231–234

Crooks GE (1999) Entropy production fluctuation theorem and the nonequilibrium work relation for free energy differences. Phys Rev E 60(3):2721–2726

Crut A, Koster DA, Seidel R, Wiggins CH, Dekker NH (2007) Fast dynamics of supercoiled DNA revealed by single-molecule experiments. Proc Natl Acad Sci USA 104(29):11957–11962

de Vlaminck I, Dekker C (2012) Recent advances in magnetic tweezers. Annu Rev Biophys 41:453–472

Dudko OK, Hummer G, Szabo A (2006) Intrinsic rates and activation free energies from single-molecule pulling experiments. Phys Rev Lett 96:108101

Dudko OK, Mathé J, Szabo A, Meller A, Hummer G (2007) Extracting kinetics from single-molecule force spectroscopy: nanopore unzipping of DNA hairpins. Biophys J 92(12):4188–4195

Dudko OK, Hummer G, Szabo A (2008) Theory, analysis, and interpretation of single-molecule force spectroscopy experiments. Proc Natl Acad Sci USA 105(41):15755–15760

Dudko OK, Mathé J, Meller A (2010) Nanopore force spectroscopy tools for analyzing single biomolecular complexes. Methods Enzym 475:565–589

Dudko OK, Graham TGW, Best RB (2011) Locating the barrier for folding of single molecules under an external force. Phys Rev Lett 107:208301

Essevaz-Roulet B, Bockelmann U, Heslot F (1997) Mechanical separation of the complementary strands of DNA. Proc Natl Acad Sci USA 94(22):11935–11940

Gittes F, Schmidt CH (1998) Signals and noise in micromechanical measurements. In: Sheetz MP (ed) Laser tweezers in cell biology, vol 55, Methods in cell biology. Academic, San Diego, pp 129–156

Gore J, Bryant Z, Nöllmann M, Le MU, Cozzarelli NR, Bustamante C (2006) DNA overwinds when stretched. Nature 442(7104):836–839

Gross P, Laurens N, Oddershede LB, Bockelmann U, Peterman EJL, Wuite GJL (2011) Quantifying how DNA stretches, melts and changes twist under tension. Nat Phys 7 (9):731–736

Gupta AN, Vincent A, Neupane K, Yu H, Wang F, Woodside MT (2011) Experimental validation of free-energy-landscape reconstruction from non-equilibrium single-molecule force spectros-copy measurements. Nat Phys 7(8):631–634

Hansen TM, Reihani SNS, Oddershede LB, Sørensen MA (2007) Correlation between mechanical strength of messenger RNA pseudoknots and ribosomal frameshifting. Proc Natl Acad Sci USA 104(14):5830–5835

Hummer G, Szabo A (2001) Free energy reconstruction from nonequilibrium single-molecule pulling experiments. Proc Natl Acad Sci USA 98(7):3658–3661

Hummer G, Szabo A (2003) Kinetics from nonequilibrium single-molecule pulling experiments. Biophys J 85(1):5–15

Hummer G, Szabo A (2010) Free energy profiles from single-molecule pulling experiments. Proc Natl Acad Sci USA 107(50):21441–21446

Iwai S, Uyeda TQP (2008) Visualizing myosin-actin interaction with a genetically-encoded fluorescent strain sensor. Proc Natl Acad Sci USA 105(44):16882–16887

Jarzynski C (1997) Nonequilibrium equality for free energy differences. Phys Rev Lett 78:2690–2693

Jin J, Bai L, Johnson DS, Fulbright RM, Kireeva ML, Kashlev M, Wang MD (2010) Synergistic action of RNA polymerases in overcoming the nucleosomal barrier. Nat Struct Mol Biol 17 (6):745–752

Junier I, Mossa A, Manosas M, Ritort F (2009) Recovery of free energy branches in single molecule experiments. Phys Rev Lett 102:070602

Keyser UF, Koeleman BN, Van Dorp S, Krapf D, Smeets RMM, Lemay SD, Dekker NH, Dekker C (2006) Direct force measurements on DNA in a solid-state nanopore. Nat Phys 2(7):473–477

Killian JL, Sheinia MY, Wang MD (2012) Recent advances in single molecule studies of nucleosomes. Curr Opin Struct Biol 22:80–87

Kruithof M, Chien FT, Routh A, Logie C, Rhodes D, van Noort J (2009) Single-molecule force spectroscopy reveals a highly compliant helical folding for the 30-nm chromatin fiber. Nat Struct Mol Biol 16(5):534–540

La Porta A, Wang MD (2004) Optical torque wrench: angular trapping, rotation, and torque detection of quartz microparticles. Phys Rev Lett 92:190801

Lavelle C, Praly E, Bensimon D, Le Cam E, Croquette V (2011) Nucleosome remodeling machines and other molecular motors observed at the single molecule level. FEBS J 298 (19):3596–3607

Leger JF, Romano G, Sarkar A, Robert J, Bourdieu L, Chatenay D, Marko JF (1999) Structural transitions of a twisted and stretched DNA molecule. Phys Rev Lett 83(5):1066–1069

Liphardt J, Onoa B, Smith SB, Tinoco I Jr, Bustamante C (2001) Reversible unfolding of single RNA molecules by mechanical force. Science 292(5517):733–737

Liphardt J, Dumont S, Smith SB, Tinoco I Jr, Bustamante C (2002) Equilibrium information from nonequilibrium measurements in an experimental test of Jarzynski's equality. Science 296:1832–1835

Mangeol P, Bizebard T, Chiaruttini C, Dreyfus M, Springer M, Bockelmann U (2011) Probing ribosomal protein–RNA interactions with an external force. Proc Natl Acad Sci USA 108 (45):18272–18276

Marko JF, Siggia ED (1995) Stretching DNA. Macromolecules 28(26):8759–8770

McNally B, Singer A, Zhiliang Y, Yingjie S, Zhipeng W, Meller A (2010) Optical recognition of converted DNA nucleotides for single-molecule DNA sequencing using nanopore arrays. NanoLetters 10:2237–2244

Minh DDL, Adib AD (2008) Optimized free energies from bidirectional single-molecule force spectroscopy. Phys Rev Lett 100(18):180602

Mossa A, de Lorenzo S, Huguet JM, Ritort F (2009) Measurement of work in single-molecule pulling experiments. J Chem Phys 130:234116

Neuman KC, Nagy A (2008) Single-molecule force spectroscopy: optical tweezers, magnetic tweezers and atomic force microscopy. Nat Methods 5(6):491–505

Oddershede LB (2012) Force probing of individual molecules inside the living cell is now a reality. Nat Chem Biol 8:879–886

Perkins T, Smith D, Chu S (1997) Single polymer dynamics in an elongational flow. Science 276 (5321):2016–2021

Ritchie DB, Foster DAN, Woodside MT (2012) Programmed -1 frameshifting efficiency correlates with RNA pseudoknot conformational plasticity, not resistance to mechanical unfolding. Proc Natl Acad Sci USA 109(40):16167–16172

Ritort F, Bustamante C, Tinoco I Jr (2002) A two-state kinetic model for the unfolding of single molecules by mechanical force. Proc Natl Acad Sci USA 99(21):13544–13548

Rohrbach A (2005) Stiffness of optical traps: quantitative agreement between experiment and electromagnetic theory. Phys Rev Lett 95:168102

Rouzina I, Bloomfield VA (2001) Force-induced melting of the DNA double helix 1. Thermodynamic analysis. Biophys J 80(2):882–893

Smith SB, Cui Y, Bustamante C (1996) Overstretching B-DNA: the elastic response of individual double stranded and single stranded DNA molecules. Science 271(5250):795–797

Stevenson DJ, Gunn-Moore F, Dholakia K (2010) Light forces the pace: optical manipulation for biophotonics. J Biomed Opt 15(2):041503

Strick T, Allemand J-F, Bensimon D, Croquette V (1998) The behavior of supercoiled DNA. Biophys J 74:2016–2028

Strunz T, Oroszlan K, Schäfer R, Güntherodt HJ (1999) Dynamic force spectroscopy of single DNA molecules. Proc Natl Acad Sci USA 96(20):11277–11282

van Mameren J, Gross P, Farge G, Hooijman P, Modesti M, Falkenberg M, Wuite GJL, Peterman EJG (2009) Unraveling the structure of DNA during overstretching by using multicolor, single-molecule fluorescence imaging. Proc Natl Acad Sci USA 106(43):18231–18236

Wang MD, Yin H, Landick R, Gelles J, Block SM (1997) Stretching DNA with optical tweezers. Biophys J 72(3):1335–1346

Williams MC, Wenner JR, Rouzina I, Bloomfield VA (2001) Effect of ph on the overstretching transition of double-stranded DNA: evidence of force-induced DNA melting. Biophys J 80 (2):874–881

Woodside MT, Behnke-Parks WM, Larizadeh K, Travers K, Herschlag D, Block SM (2006) Nanomechanical measurements of the sequence-dependent folding landscapes of single nucleic acid hairpins. Proc Natl Acad Sci USA 103(16):6190–6195

Zhang X, Chen H, Fu H, Doyle PS, Yan J (2012) Two distinct overstretched DNA structures revealed by single-molecule thermodynamics measurements. Proc Natl Acad Sci USA 109 (21):8103–8108